Electronic Supplementary Material (ESI) for CrystEngComm.

Electronic Supplementary Information

Two interpenetrated metal-organic frameworks with a slim ethynyl-based ligand: designed for selective gas adsorption and structural tuning

Xiang-Jing Kong, Yong-Zheng Zhang, Tao He, Xue-Qian Wu, Ming-Ming Xu, Si-Nan Wang, Lin-Hua Xie, Jian-Rong Li*

† *Beijing Key Laboratory for Green Catalysis and Separation, Department of Chemistry and Chemical Engineering, College of Environmental and Energy Engineering, Beijing University of Technology, Beijing 100124, P. R. China.*

E-mail: jrli@bjut.edu.cn

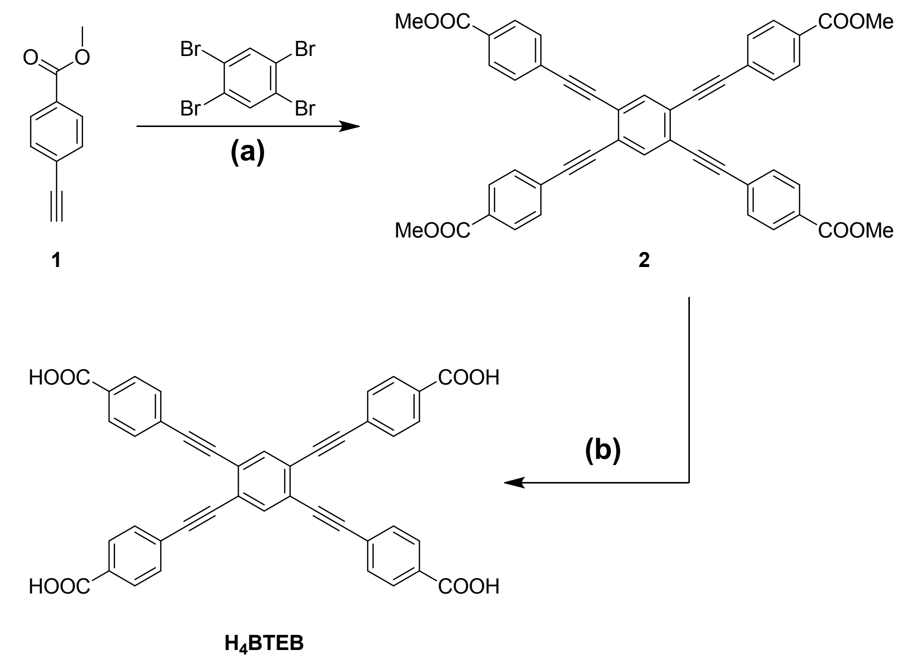

Scheme S1. The synthesis of ligand **H_4BTEB**: (a) $Pd(PPh_3)_2Cl_2$, CuI, PPh_3, Et_3N, THF/H_2O, 70 °C, 48 h; and (b) NaOH, THF/MeOH/H_2O, 70 °C, 24 h.

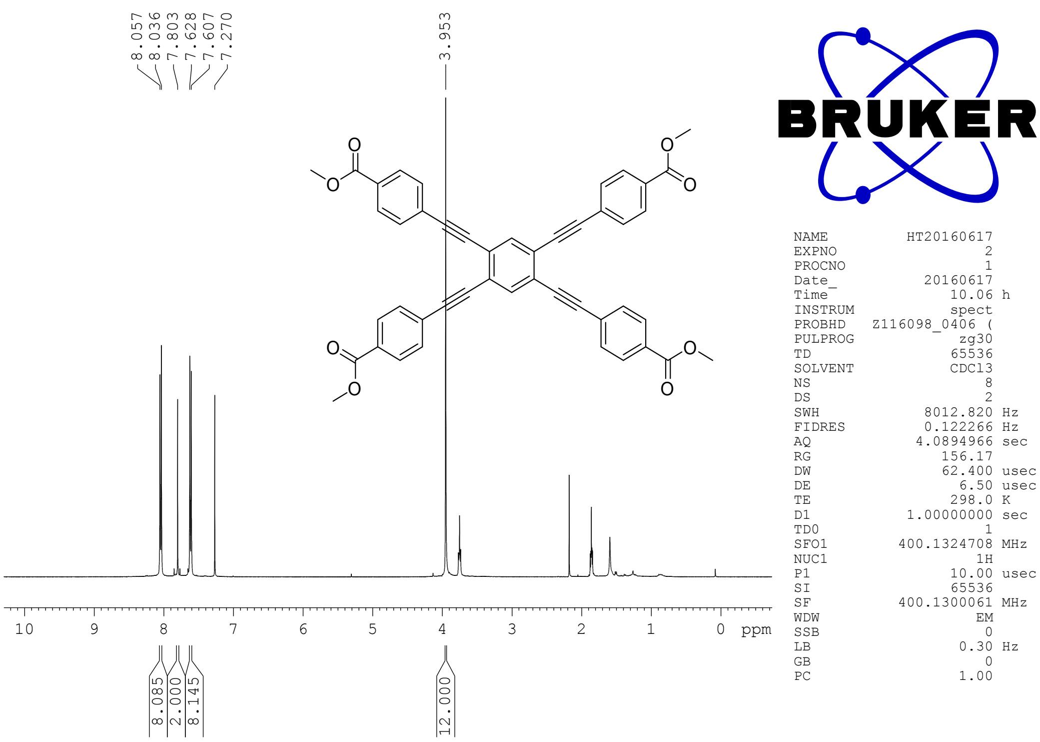

Fig. S1. ^{1}H NMR spectrum of **2**.

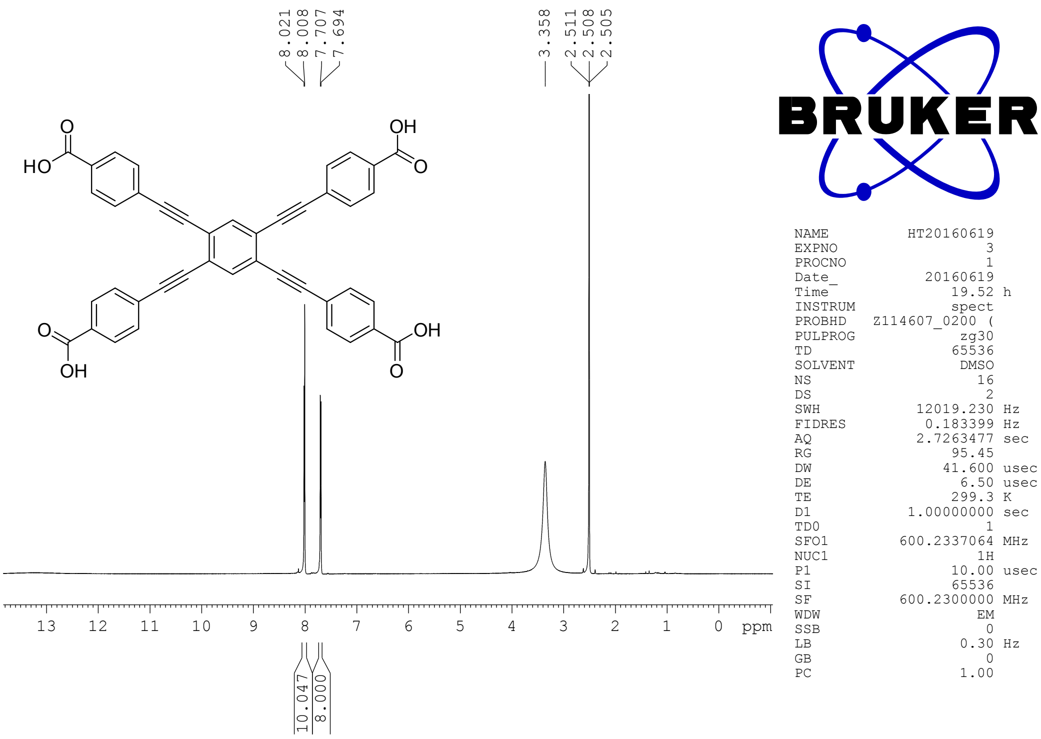

Fig. S2. ^{1}H NMR spectrum of **H_4BTEB**.

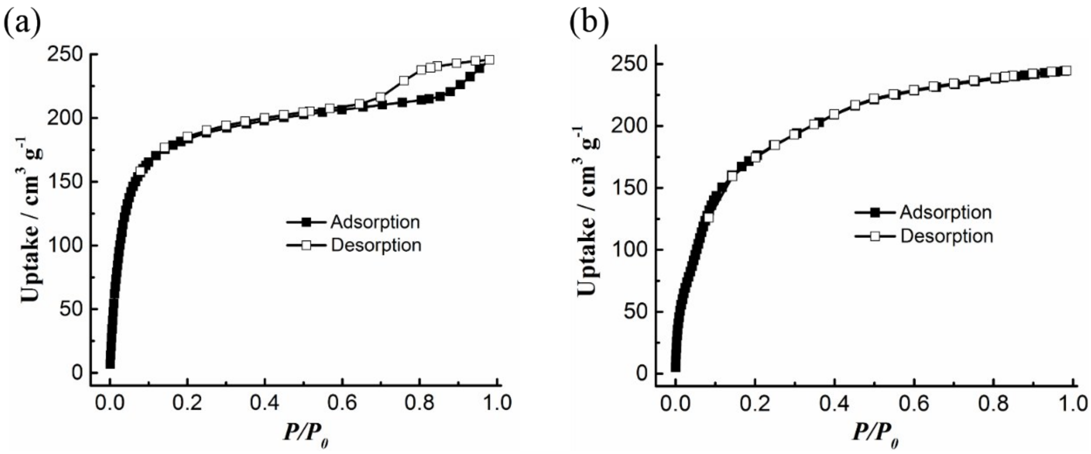

Fig. S3. CO_2 sorption isotherms at 195 K for BUT-43 (a) and BUT-44 (b).

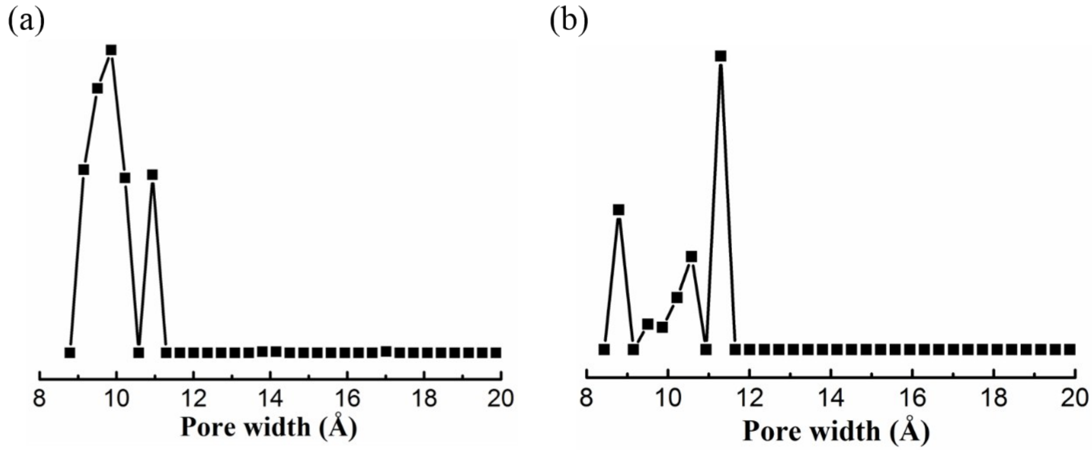

Fig. S4. Pore size distributions evaluated by using the N_2 adsorption data for BUT-43 (a) and BUT-44 (b).

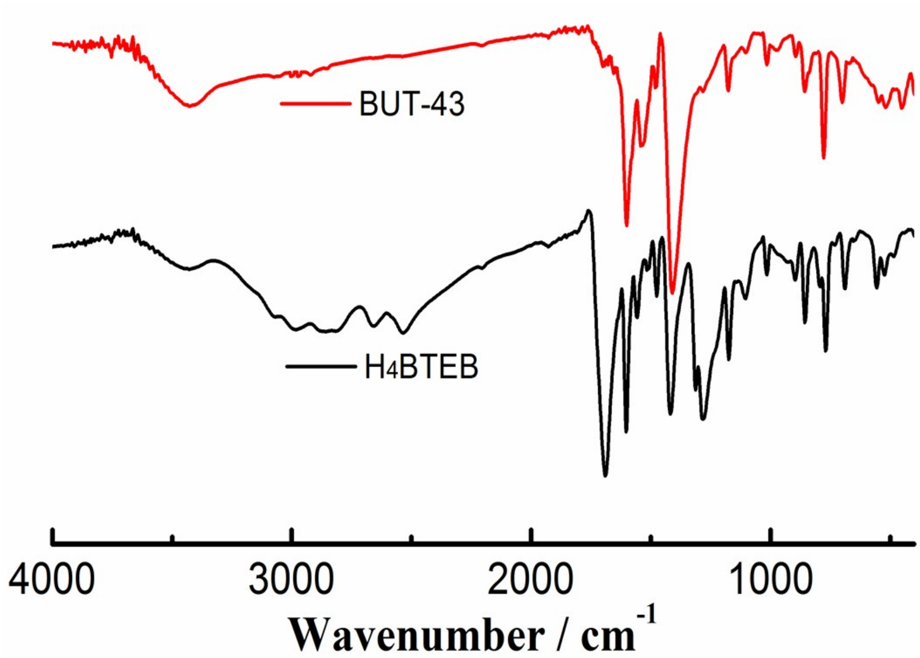

Fig. S5. FT-IR spectra of H_4BTEB and BUT-43.

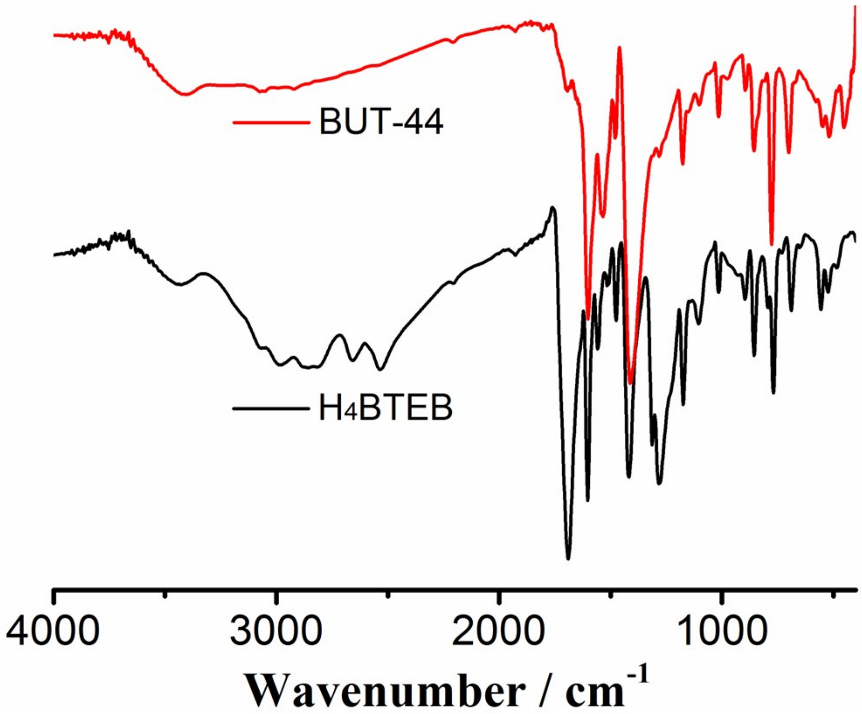

Fig. S6. FT-IR spectra of H_4BTEB and BUT-44.

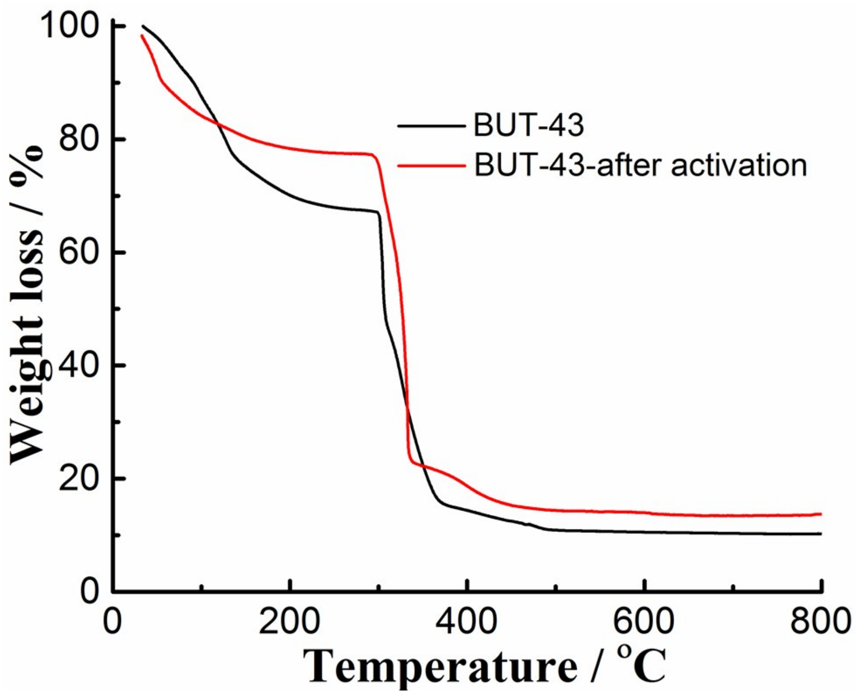

Fig. S7. TGA curves of BUT-43.

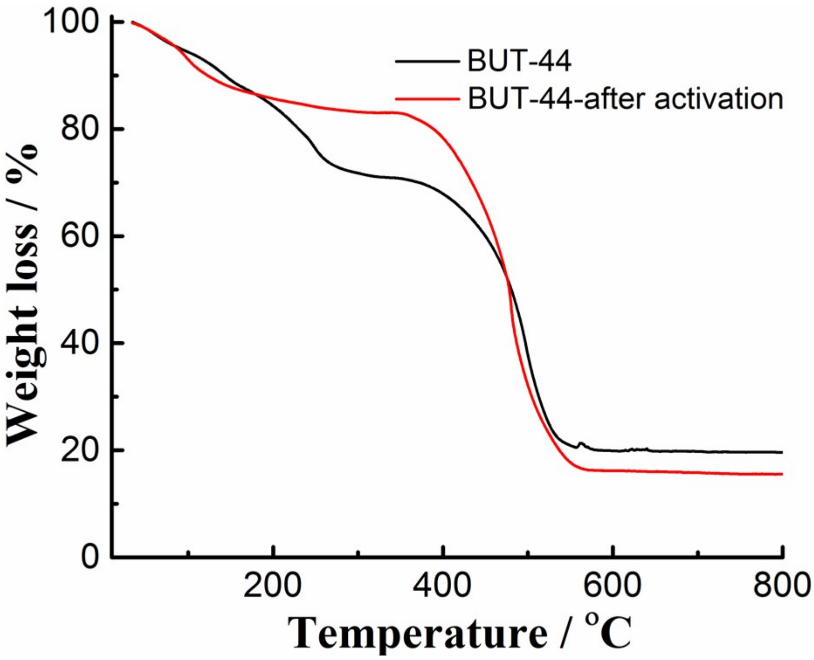

Fig. S8. TGA curves of BUT-44.

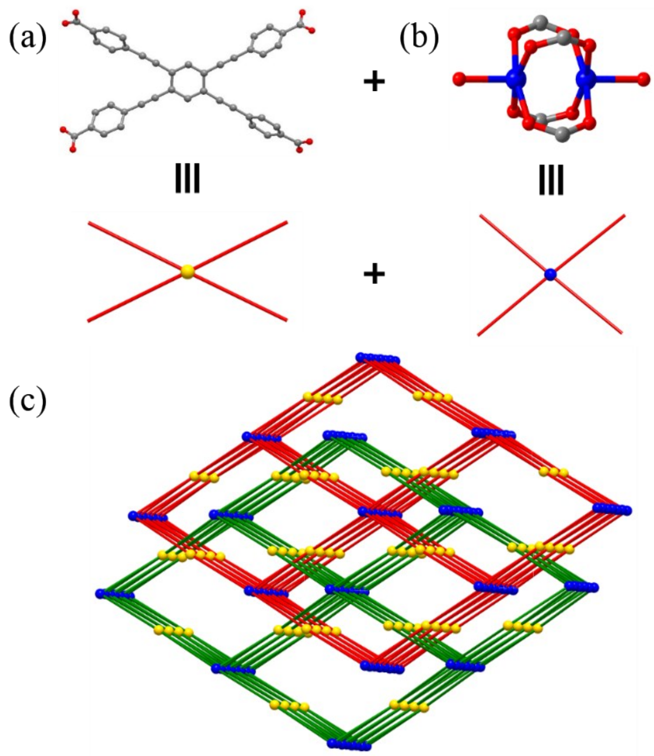

Fig. S9. Topological network representations of the ligand $BTEB^{4-}$ (a), 4-connected Cu_2 cluster (b), and two-fold interpenetrated 4-connected network of BUT-43 (c).

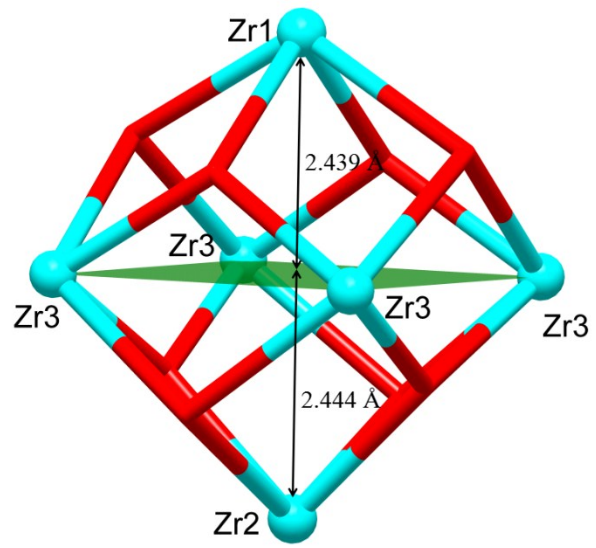

Fig. S10. The slightly deformed Zr_6 cluster in BUT-44.

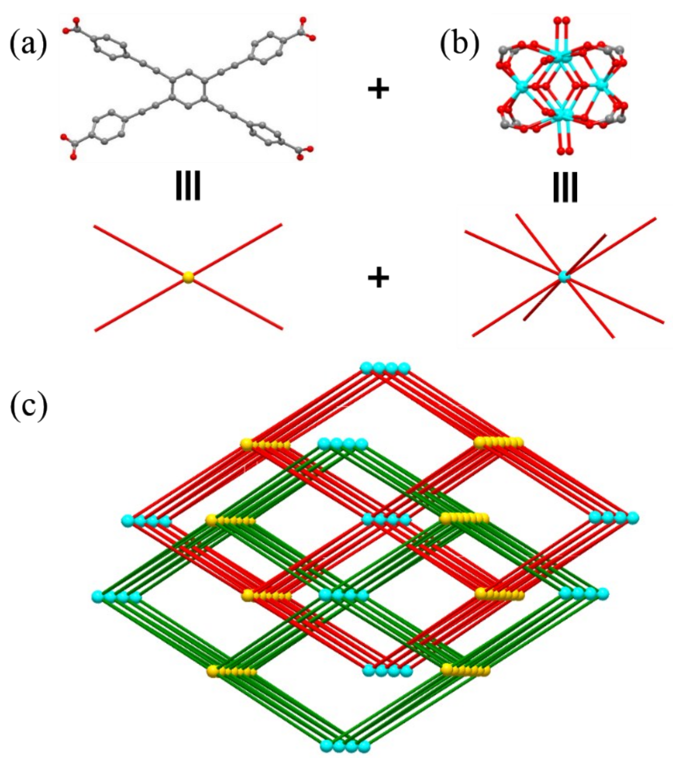

Fig. S11. Topological network representations of the ligand $BTEB^{4-}$ (a), Zr_6 cluster (b), and two-fold interpenetrated 4,8-connected network of BUT-44 (c).

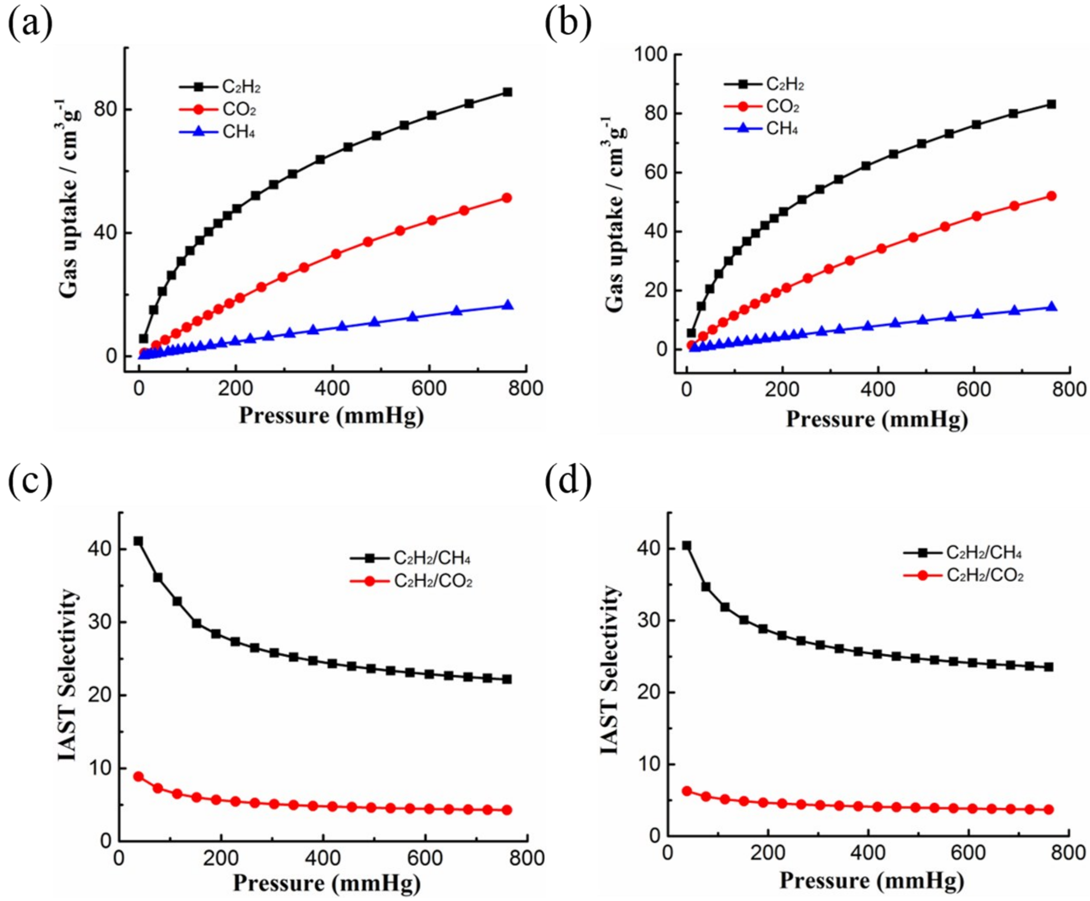

Fig. S12. C_2H_2, CO_2, and CH_4 adsorption isotherms recorded at 273 K for BUT-43 (a) and -44 (b); IAST C_2H_2/CH_4 and C_2H_2/CO_2 selectivities in BUT-43 (c) and BUT-44 (d) at 273 K.

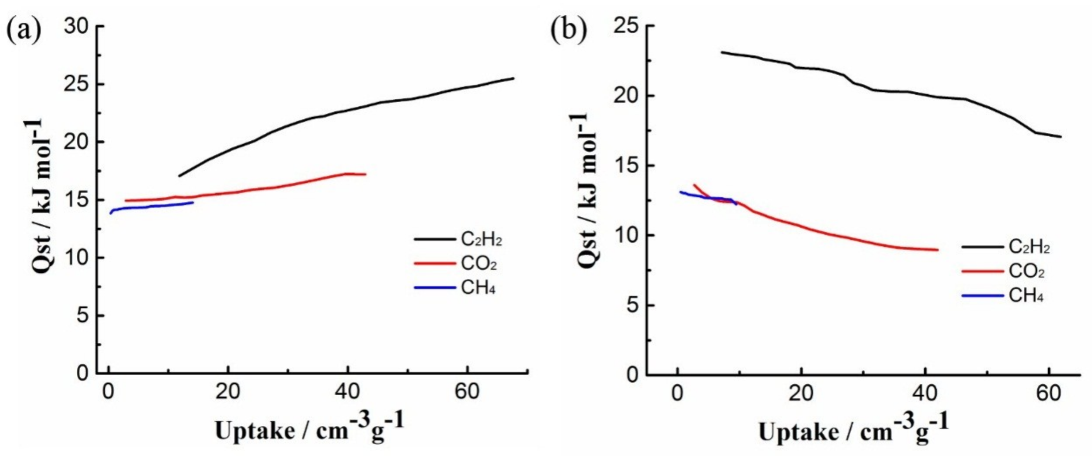

Fig. S13. The isosteric heats of adsorption (Qst) of C_2H_2, CO_2, and CH_4 in BUT-43 (a) and BUT-44 (b).

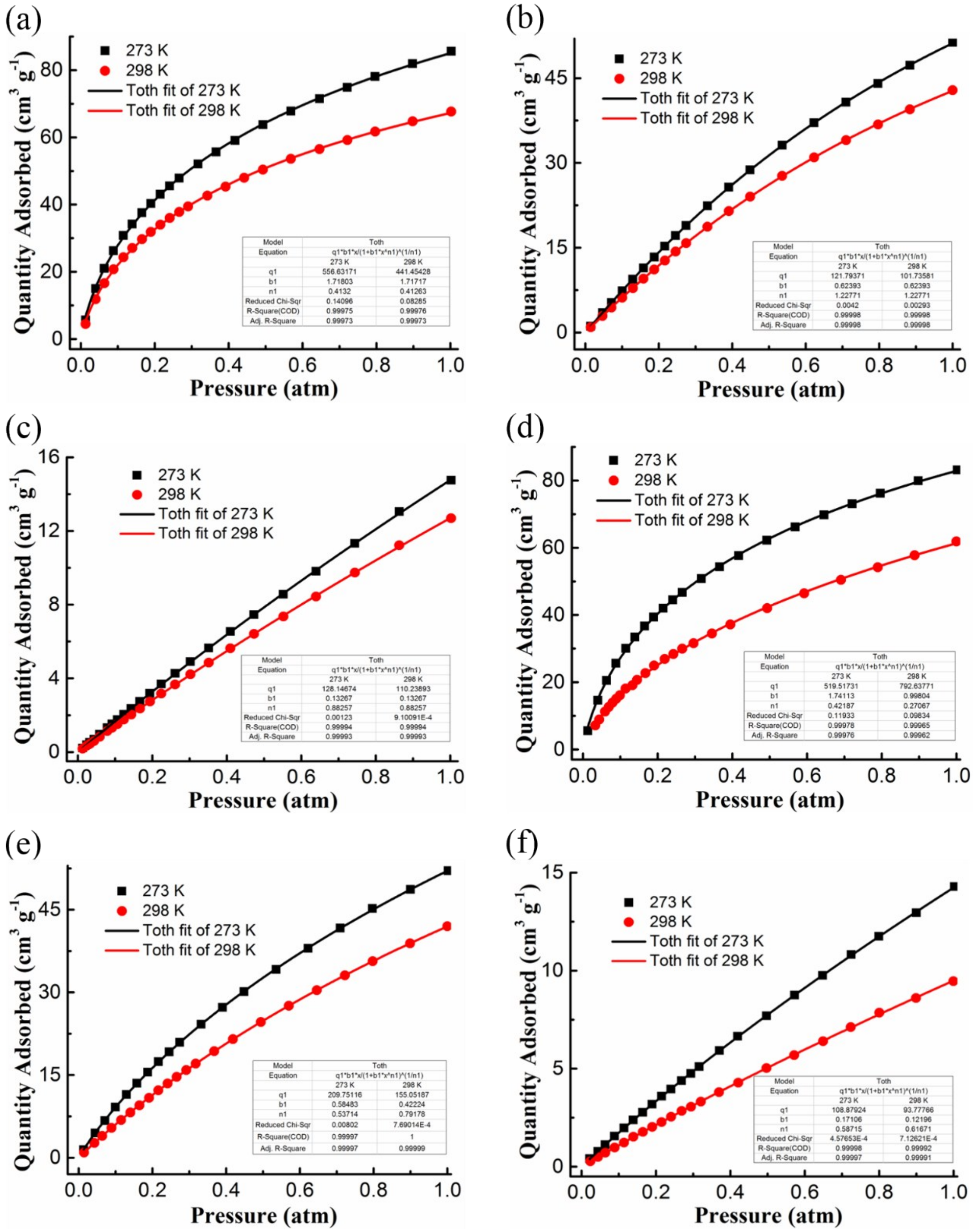

Fig. S14. C_2H_2 (a) CO_2 (b) CH_4 (c) adsorption isotherms of BUT-43 and C_2H_2 (d) CO_2 (e) CH_4 (f) of BUT-44 measured at 273 and 298 K, and their Toth fits.

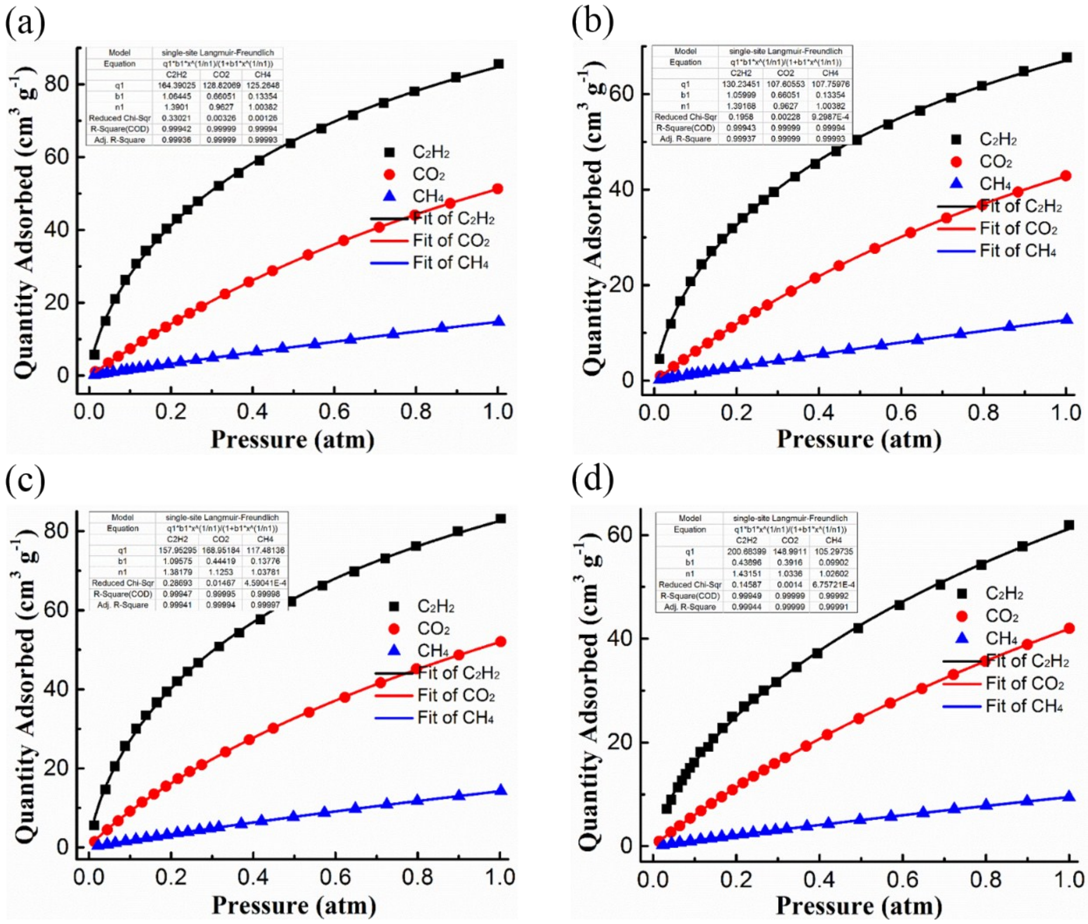

Fig. S15. C_2H_2, CO_2 and CH_4 adsorption isotherms of BUT-43 at 273K (a) and 298 K (b) and of BUT-44 at 273K (c) and 298 K (d), and their single-site Langmuir-Freundlich isotherm fits.

Table S1. The crystallographic data and structure refinement for BUT-43.

Formula	$C_{42}H_{22}Cu_2O_{10}$
M	813.67
Crystal system	monoclinic
Space group	*C*2/*c*
a/ Å	42.7196(15)
b/ Å	23.6272(18)
c/ Å	21.5936(9)
α/ °	90
β/ °	120.317(4)
γ/ °	90
V/ $Å^3$	18814.8(19)
Z	8
D_C /g cm^{-3}	0.575
μ /mm^{-1}	0.756
T/ K	100.01(10)
Reflections collected	30784
Independent reflections	14747 [R_{int} = 0.0970, R_{sigma} = 0.1321]
Goodness-of-fit on F^2	1.040
R_1^a, wR_2^b [$I > 2\sigma(I)$]	R_1 = 0.0991, wR_2 = 0.2629
R_1^a, wR_2^b (all data)	R_1 = 0.1478, wR_2 = 0.2937
Largest diff. peak and hole (e.$Å^{-3}$)	0.61 / –0.63

$R_1^a = \Sigma||F_o|-|F_c|| / \Sigma|F_o|$

$wR_2^b = \{\Sigma[w(F_o^2-F_c^2)^2]/[w(F_o^2)^2]\}^{1/2}$, $[F_o > 4\sigma(F_o)]$

Table S2. The crystallographic data and structure refinement for BUT-44.

Formula	$C_{42}H_{26}O_{16}Zr_3$
M	1060.22
Crystal system	orthorhombic
Space group	*Cmcm*
a/ Å	25.068(5)
b/ Å	42.667(2)
c/ Å	13.8078(11)
α/ °	90
β/ °	90
γ/ °	90
V/ Å^3	14768(3)
Z	8
D_C /g cm^{-3}	0.946
μ /mm^{-1}	3.768
T/ K	100.01(10)
Reflections collected	15455
Independent reflections	6978 [R_{int} = 0.0755, R_{sigma} = 0.0984]
Goodness-of-fit on F^2	0.943
R_1^a, wR_2^b [$I > 2\sigma(I)$]	R_1 = 0.0711, wR_2 = 0.1909
R_1^a, wR_2^b (all data)	R_1 = 0.1010, wR_2 = 0.2160
Largest diff. peak and hole (e.Å^{-3})	1.30 / –1.53

$R_1^a = \Sigma||F_o|-|F_c|| / \Sigma|F_o|$

$wR_2^b = \{\Sigma[w(F_o^2-F_c^2)^2]/[w(F_o^2)^2]\}^{1/2}$, $[F_o>4\sigma(F_o)]$